Supplementary Information for

Overcoming insecticide resistance through computational inhibitor design

Galen J. Correy, Daniel Zaidman, Alon Harmelin, Silvia Carvalho, Peter D. Mabbitt, Viviane Calaora, Peter J. James, Andrew C. Kotze, Colin J. Jackson* and Nir London*

Corresponding authors: Colin J. Jackson and Nir London and
Email: colin.jackson@anu.edu.au or nir.london@weizmann.ac.il

This PDF file includes:

Figures S1 to S22
Tables S1 to S5
SI References

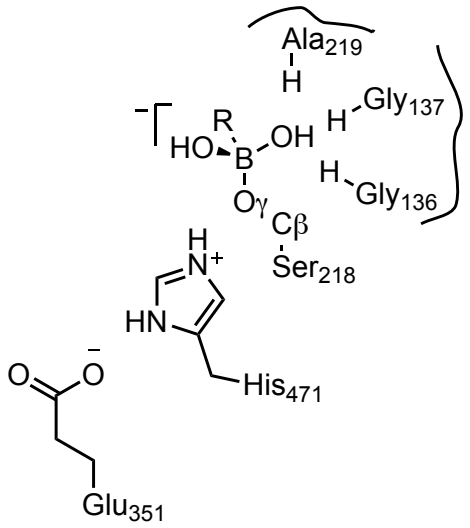

Figure S1. Orientation of boronic acids used for virtual screen. The boronic acids were covalently attached to the catalytic serine (Ser218) of *Lc*αE7. The catalytic histidine (His471) was represented in its doubly protonated form. The B-Oγ bond was set to 1.5 ± 0.1 Å and the Cβ-Oγ-B bond angle was set to 116.0 ± 5° and the Oγ-B-R bond angle was set to 109.5 ± 5°. In the manual selection of compounds for testing, preference was given to compounds where either of the boronic acid hydroxyls occupied the oxyanion hole (formed by the backbone nitrogens of Gly136, Gly137 and Ala219).

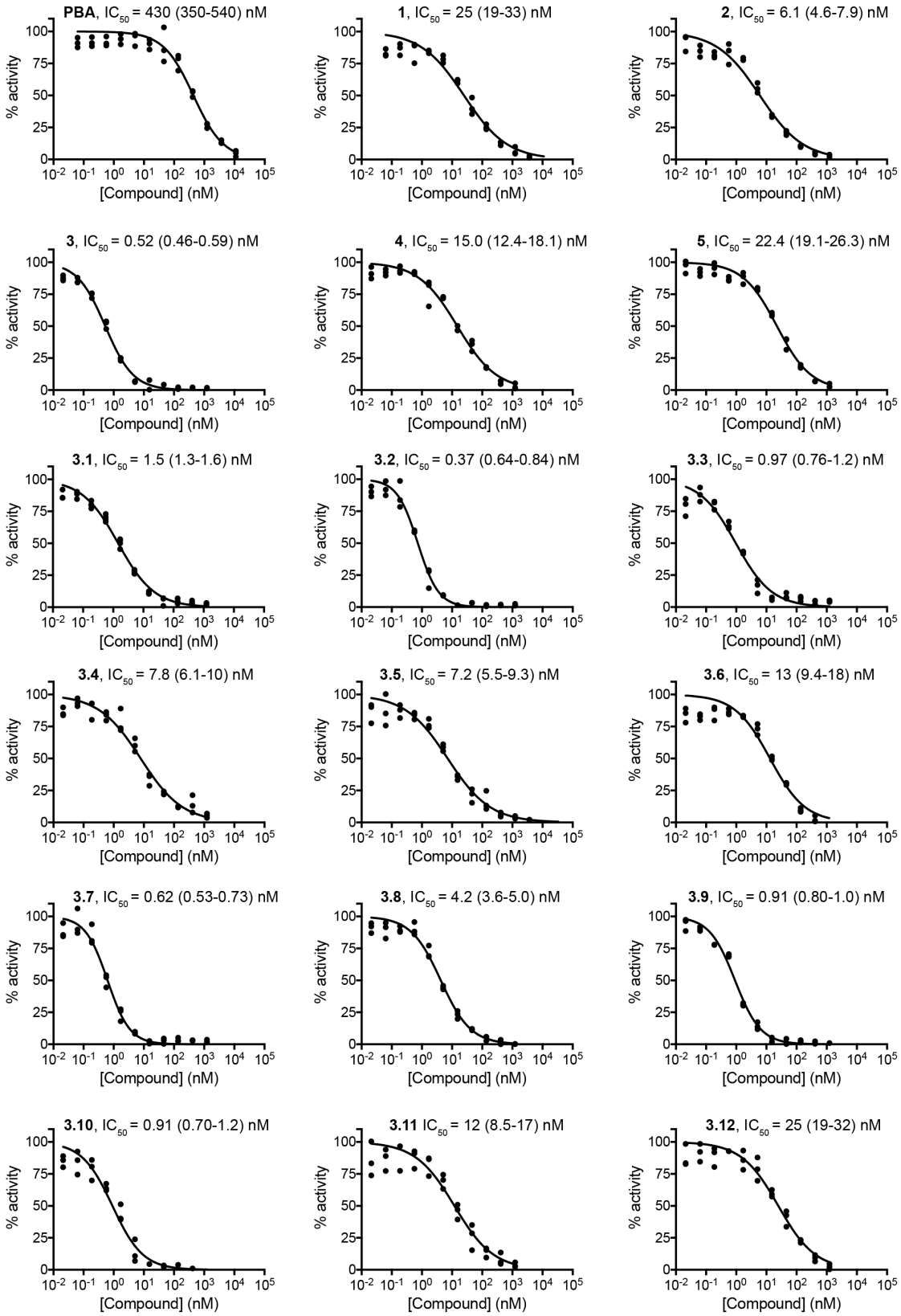

Figure S2. Dose-response curves for the inhibition of wild type *Lc*α*E7*. Inhibition of the hydrolysis of 4-nitrophenyl was determined for phenylboronic acid (PBA) and compounds **1**-**5** and **3.1**-**3.12**. Three repeat measurements of enzyme activity were performed for each concentration of boronic acid. The concentration of boronic acid required to inhibit 50% of activity (IC_{50}) was determined by fitting a sigmoidal dose-response curve to plots of percentage inhibition. The curve was constrained to 0 (bottom) and 100% (top) inhibition with a variable Hill slope. IC_{50} values are quoted with the 95% confidence interval.

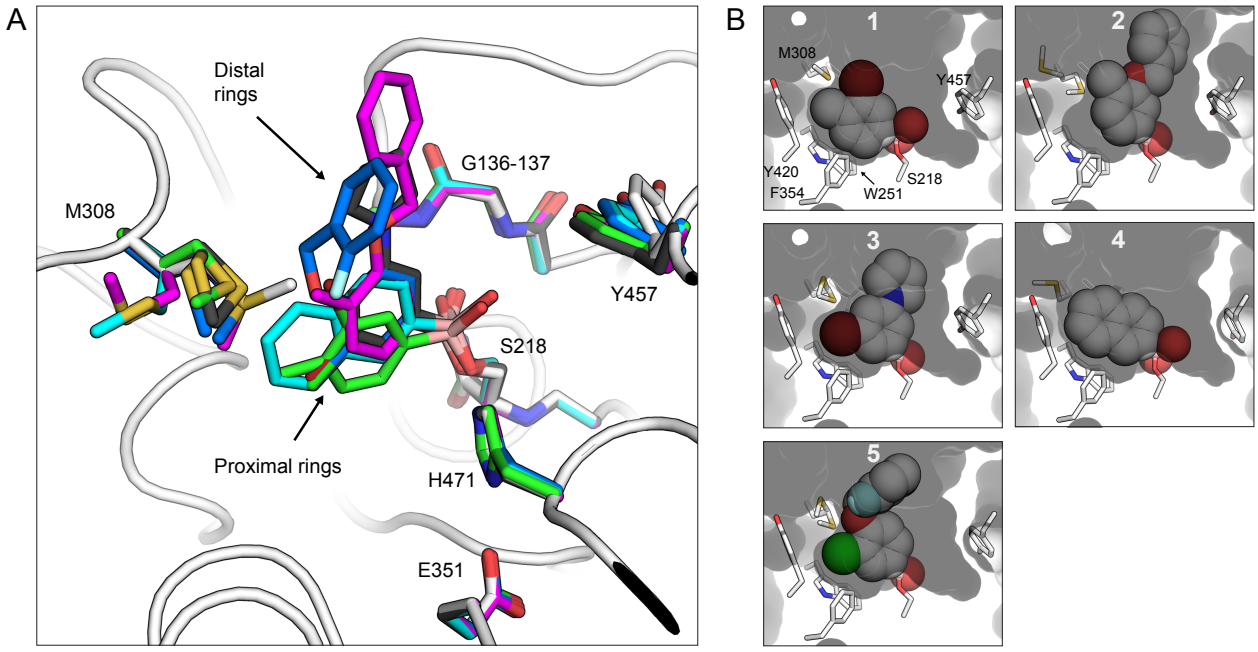

Figure S3. Structural features of compounds 1-5 binding to wild type *Lc*αE7. *(A)* Overlay of the five wild type *Lc*αE7 co-crystal structures. The key amino acid side chains and the covalently bound boronic acids are shown as sticks coloured by inhibitor: apo = white, **1** = green, **2** = magenta, **3** = black, **4** = cyan and **5** = blue. The boronic acids occupy the larger of the two *Lc*αE7 binding pocket subsites, which accommodates a fatty acid chain of the predicted native lipid substrate (1). The distal rings of compounds **2**, **3** and **5** are projected toward the funnel that leads to the active site. There is minor structural rearrangement in the enzyme-inhibitor complexes with the geometry of the oxyanion hole, and hydrogen bonding within the catalytic triad, remaining intact. Structural differences includes rotation of the Tyr457 side chain, which occludes the smaller subsite of the *Lc*αE7 binding pocket, and has previously been noted to occur upon OP binding (2), and changes in the position of the Met308 side-chain. *(B)* Surface representation of *Lc*αE7 binding pocket with compounds **1**-**5** shown as spheres.

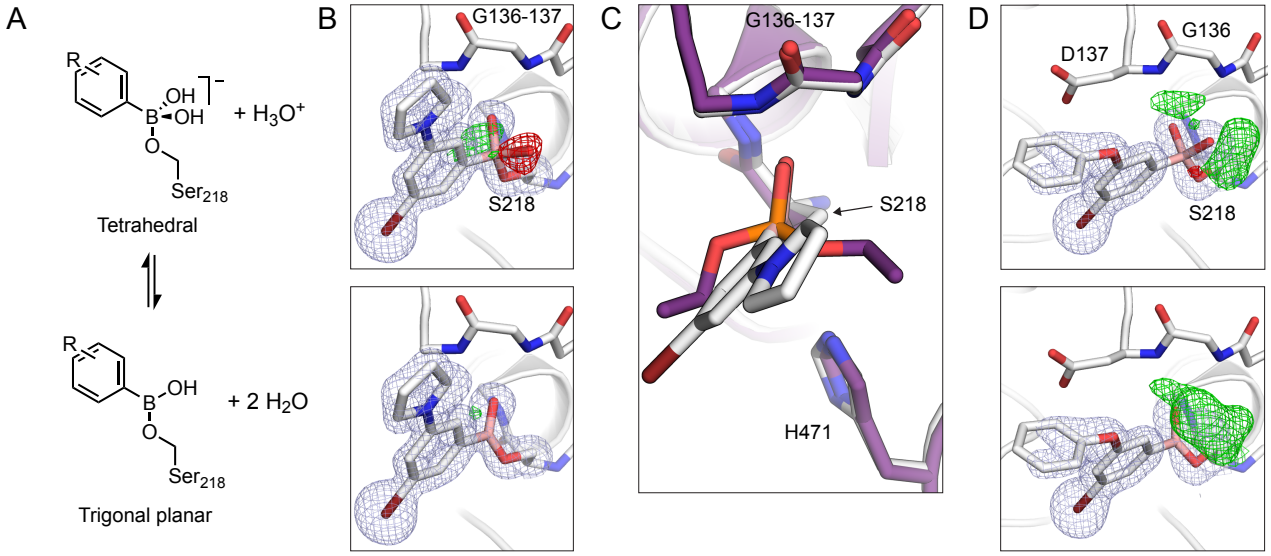

Figure S4. Boronic acids adopt both tetrahedral and trigonal planar geometries when coordinated to the catalytic serine of *Lc*αE7. *(A)* Chemical structures of tetrahedral and trigonal planar boronic acid adducts. The tetrahedral geometry is frequently invoked to rationalize high affinity binding of boronic acid compounds to serine hydrolyase (3–8). To our knowledge, there has only been a single report of a trigonal planar adduct (9). *(B)* Compound **3** formed a trigonal planar adduct when bound to wild type *Lc*αE7. Geometry was assigned with reference to the positive (green mesh) and negative (red mesh) peaks in the mF_O-DF_C difference electron density (contoured at ±3 σ) with either the tetrahedral (top) or trigonal planar (bottom) adducts modelled. The ligand and selected active site residues are shown as white sticks, with $2mF_O$-DF_C electron density (blue mesh) contoured at 1 σ. Analysis of the difference density of the other compounds indicates that compounds **2** and **5** also formed trigonal planar adducts, while compounds **1** and **4** formed tetrahedral adducts. Hydrogen bonds to the oxyanion hole were shorter for the trigonal planar adducts; the average distance was 2.7 Å for trigonal planar (compounds **2**, **3** and **5**) versus 3.0 Å for the tetrahedral (compounds **1** and **4**). *(C)* The trigonal planar adduct of compound **3** (white sticks) occupies the oxyanion hole in a similar manner compared to a bound diethyl OP (purple sticks). *(D)* Difference electron density (mF_O-DF_C contoured at ±3 σ) suggests that compound **3.10** forms a tetrahedral adduct when bound to Gly137Asp *Lc*αE7.

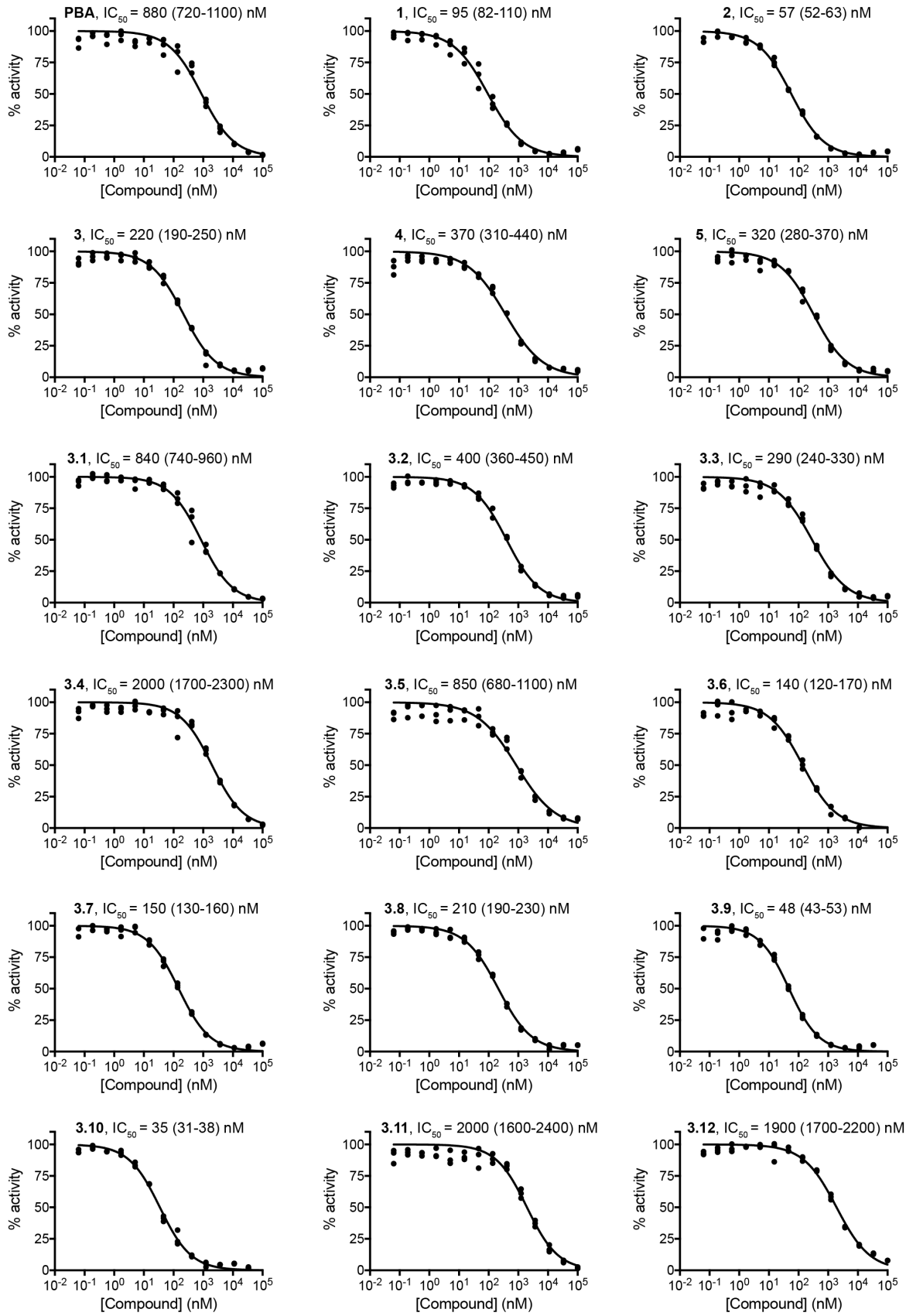

Figure S5. Dose-response curves for the inhibition of Gly137Asp *Lc*αE7**.** Inhibition of the hydrolysis of 4-nitrophenyl was determined for phenyl boronic acid (PBA) and compounds **1**-**5** and **3.1**-**3.12**. Repeats and analysis was the same as Fig S2.

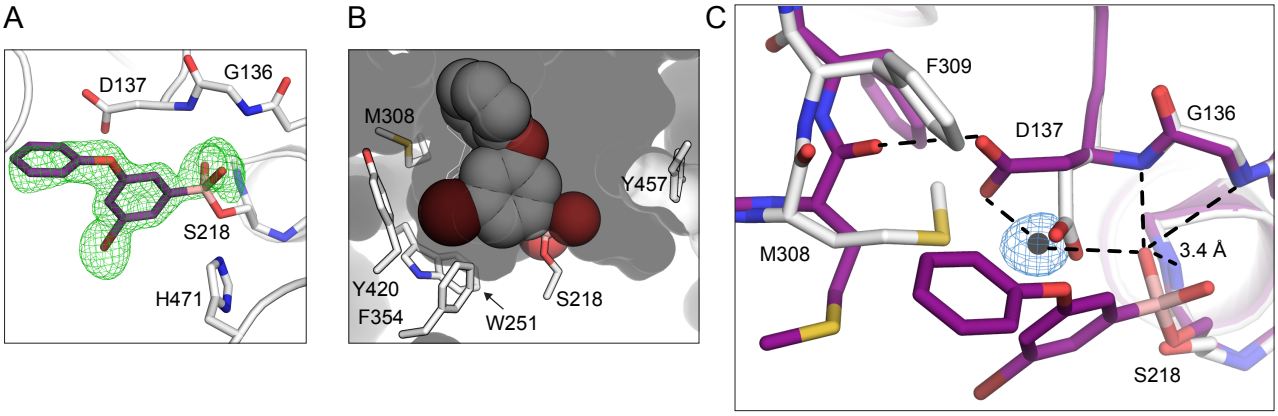

Figure S6. Rearrangement of the active site upon compound 3.10 binding to Gly137Asp *Lc*αE7. *(A)* Omit density (green mesh contoured at 3 σ) showing **3.10** covalently bound to the catalytic serine (Ser218). *(B)* Compound **3.10** binding to the Gly137Asp *Lc*αE7 mutant is conserved relative to the wild type enzyme (see Fig. S2). *(C)* Rearrangement of the Gly137Asp *Lc*αE7 active site upon with **3.10** binding. The co-crystal structure of compound **3.10** (purple sticks, PDB code 5TYJ) is overlaid with the apo Gly137Asp *Lc*αE7 structure (white sticks, PDB code 5C8V). To accommodate the covalently bound inhibitor, the side chains of Asp137, Met308 and Phe309 adopt new, alternative conformations. This rearrangement is consistent with molecular dynamics simulations of *Lc*αE7 which suggest that this conformational sub-state could be sampled by the free enzyme (10), and indicates that, like OPs, binding of the boronic acid **3.10** to *Lc*αE7 involves binding to minor conformational sub-states of the *Lc*αE7 active site. This rearrangement forms a new network of hydrogen bonds which connects the Met308 backbone with the bound inhibitor via the Asp137 carboxylate and a water molecule. Hydrogen bonds are shown as dashed black lines. All hydrogen bonds are 2.8 Å except for the Gly136 N to boronic acid OH which is 3.4 Å. The water molecule mediating a hydrogen bond between the Asp137 sidechain and the boronic acid is shown as a black sphere with $2mF_O$-DF_C electron density (contoured at 1 σ).

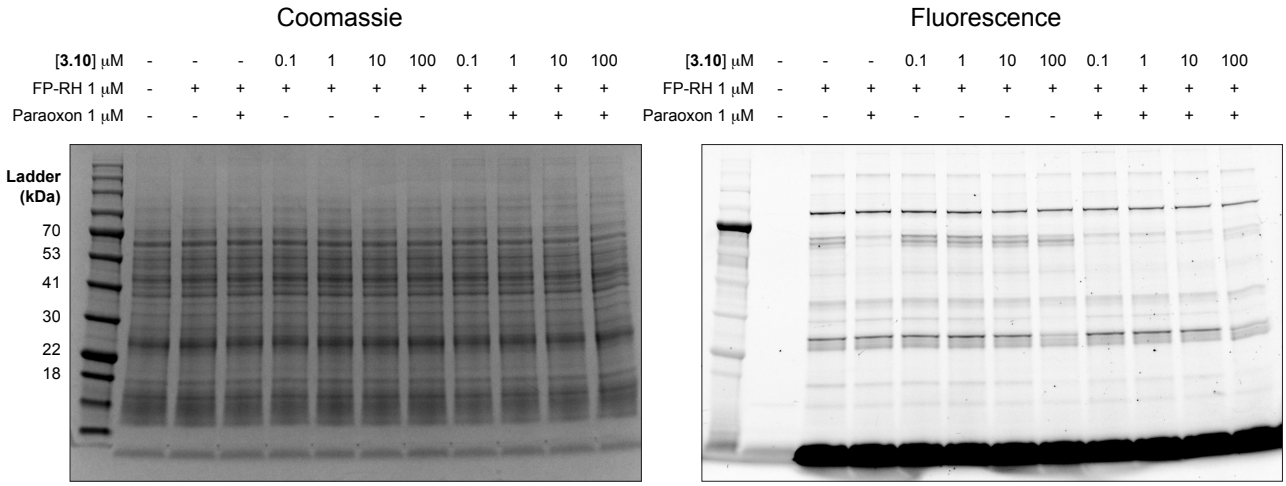

Figure S7. In-gel activity-based protein profiling of serine hydrolases in *L. cuprina* lysate. Cell lysates were incubated with a fluorophosphonate-rhodamine (FP-RH) probe, that potently and non-specifically labels serine hydrolases, with or without pre-incubation of compound **3.10** or paraoxon (10 minutes; 37°C). The two images are of the same gel visualized with visible light (left), showing all proteins, and fluorescence (right), showing only proteins labelled with the FP-RH probe.

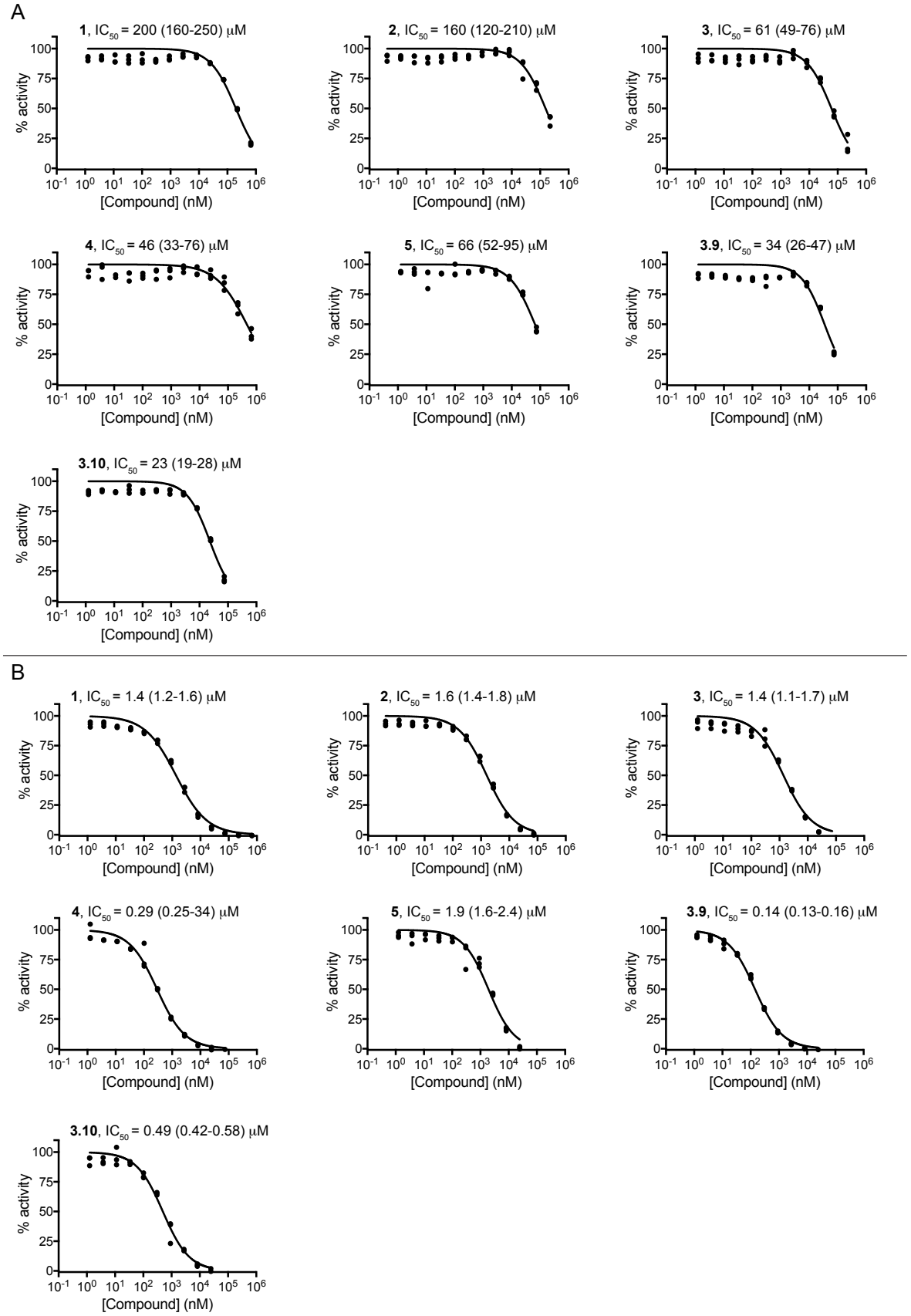

Figure S8. Dose-response curves for the inhibition of human acetylcholinesterase *(A)* and butyrylcholinesterase *(B)*. Inhibition of the hydrolysis of acetylthiocholine / butyrylthiocholine was determined for compounds **1**-**5** and **3.9**-**3.10**. Repeats and analysis were the same as Fig S2.

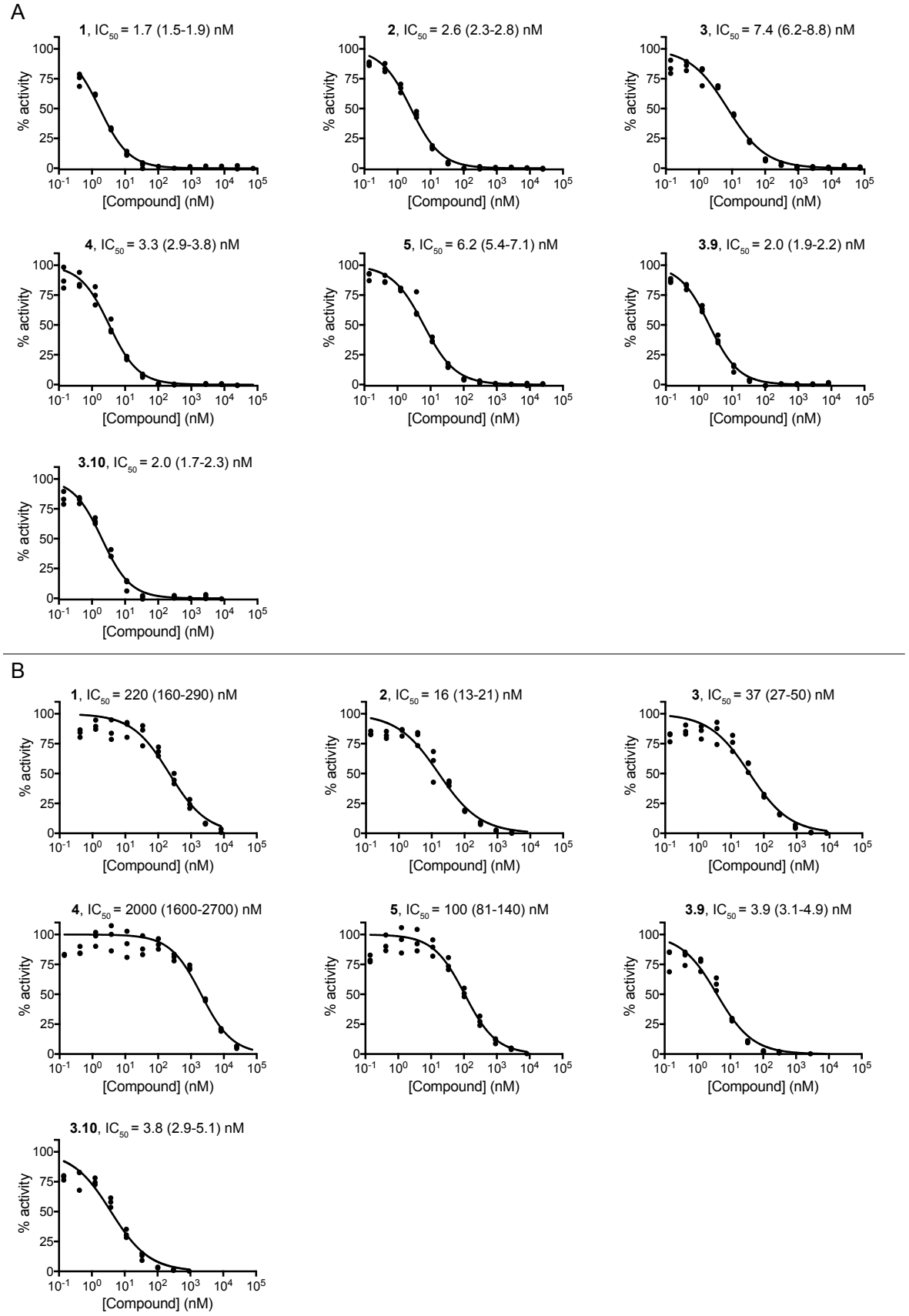

Figure S9. Dose-response curves for the inhibition of human carboxylesterase 1 *(A)* and carboxylesterase 2 *(B)*. Inhibition of the hydrolysis of 4-nitrophenyl acetate was determined for compounds **1**-**5** and **3.9**-**3.10**. Repeats and analysis were the same as Fig S2.

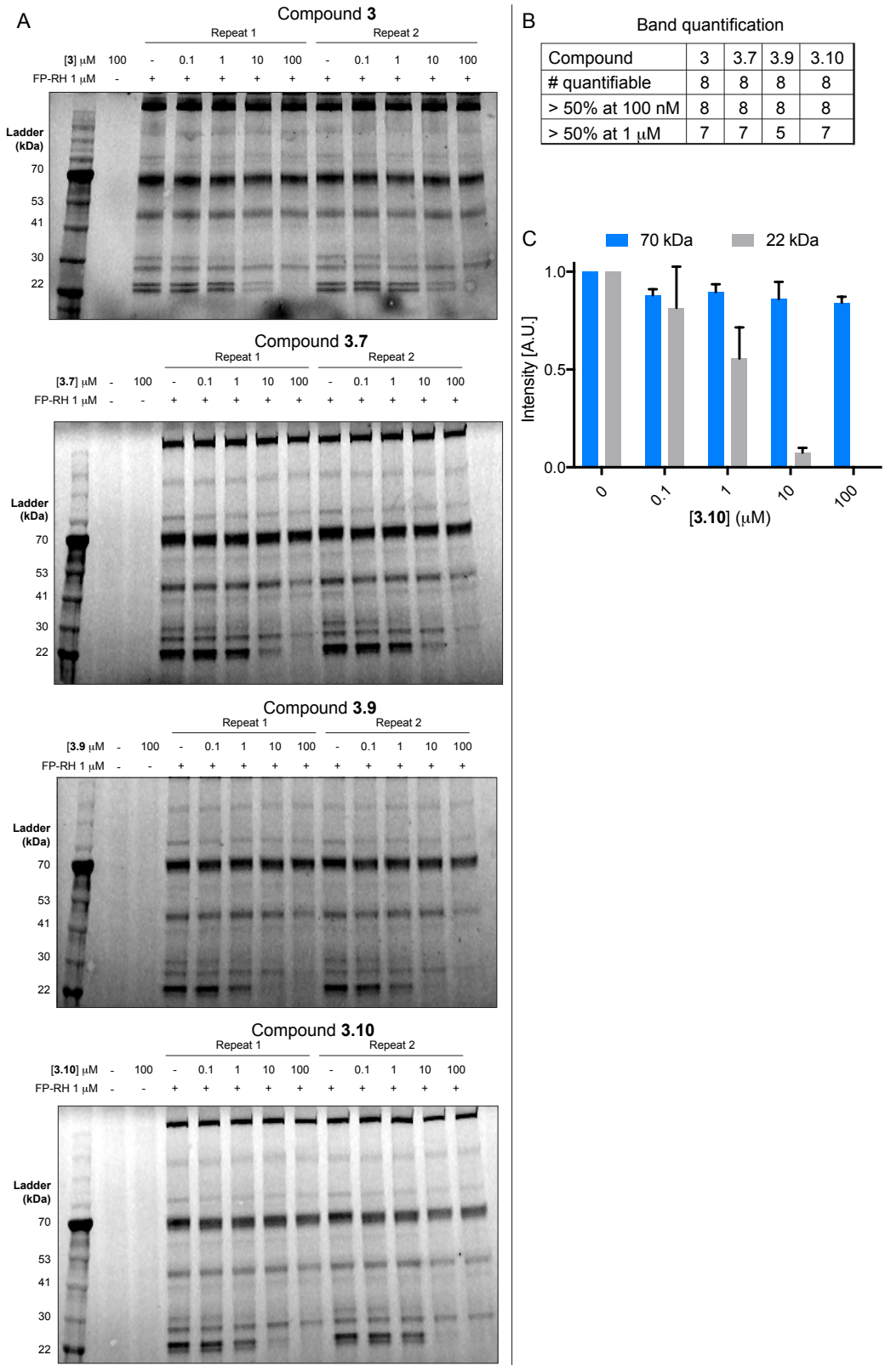

Compound	3	3.7	3.9	3.10
# quantifiable	8	8	8	8
> 50% at 100 nM	8	8	8	8
> 50% at 1 μM	7	7	5	7

Figure S10. Summary of in-gel fluorescence activity-based protein profiling of serine hydrolases with HEK cell lysate. *(A)* Cell lysates were incubated with a fluorophosphonate-rhodamine (FP-RH) probe, that potently and non-specifically labels serine hydrolases, with or without pre-incubation of the four indicated boronic acids (**3**, **3.7**, **3.9**, **3.10**; 10 minutes; 37°C) at increasing concentrations (0.1, 1, 10, 100 μM). *(B)* Summary of the number of quantifiable serine hydrolase bands from gels shown in *(A)*. Of the eight quantifiable bands, none were diminished by more than 50% with 100 nM of any of the four tested compounds. *(C)* Quantification of the two indicated bands for compound **3.10**. Error bars show standard deviation from three biological repeats.

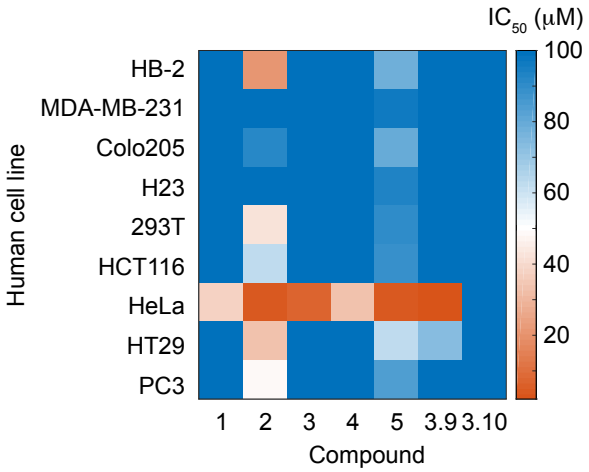

Figure S11. Boronic acid compounds display low toxicity against human cell lines. Heat-map showing the concentration of compounds required to inhibitor cell growth of a given cell line by 50%. The compounds were incubated with cells for 48 h and cell viability was measured using a cell luminescence assay. The dose-response curves used to calculate IC_{50} values are shown in Fig. S12 and S13.

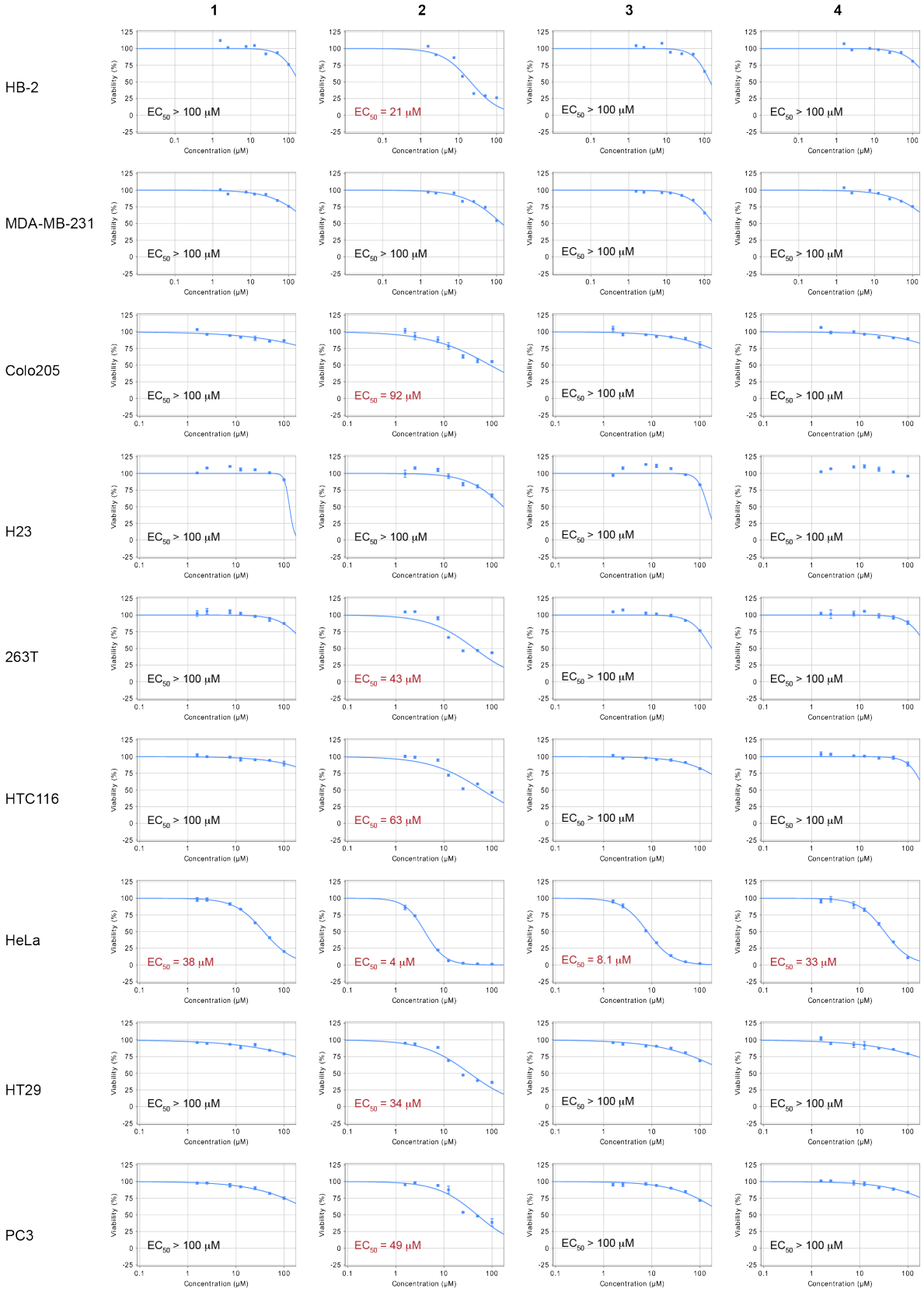

Figure S12. Boronic acids compounds **1**-**4** show little cell toxicity except against HeLa cells. Compounds were incubated for 48 h with seven human cell lines at seven concentrations up to 100 μM. Cell viability was measured after 48 h using Cell-Titer-Glo assay. The best-fit EC_{50} values are quoted on each plot for single measurements at each concentration for HB-2 and MDA-MB-231 cell lines, and duplicate measurements for the remaining seven cell lines. The cell toxicity for compounds **5**, **3.9** and **3.10** is shown in Fig. S13.

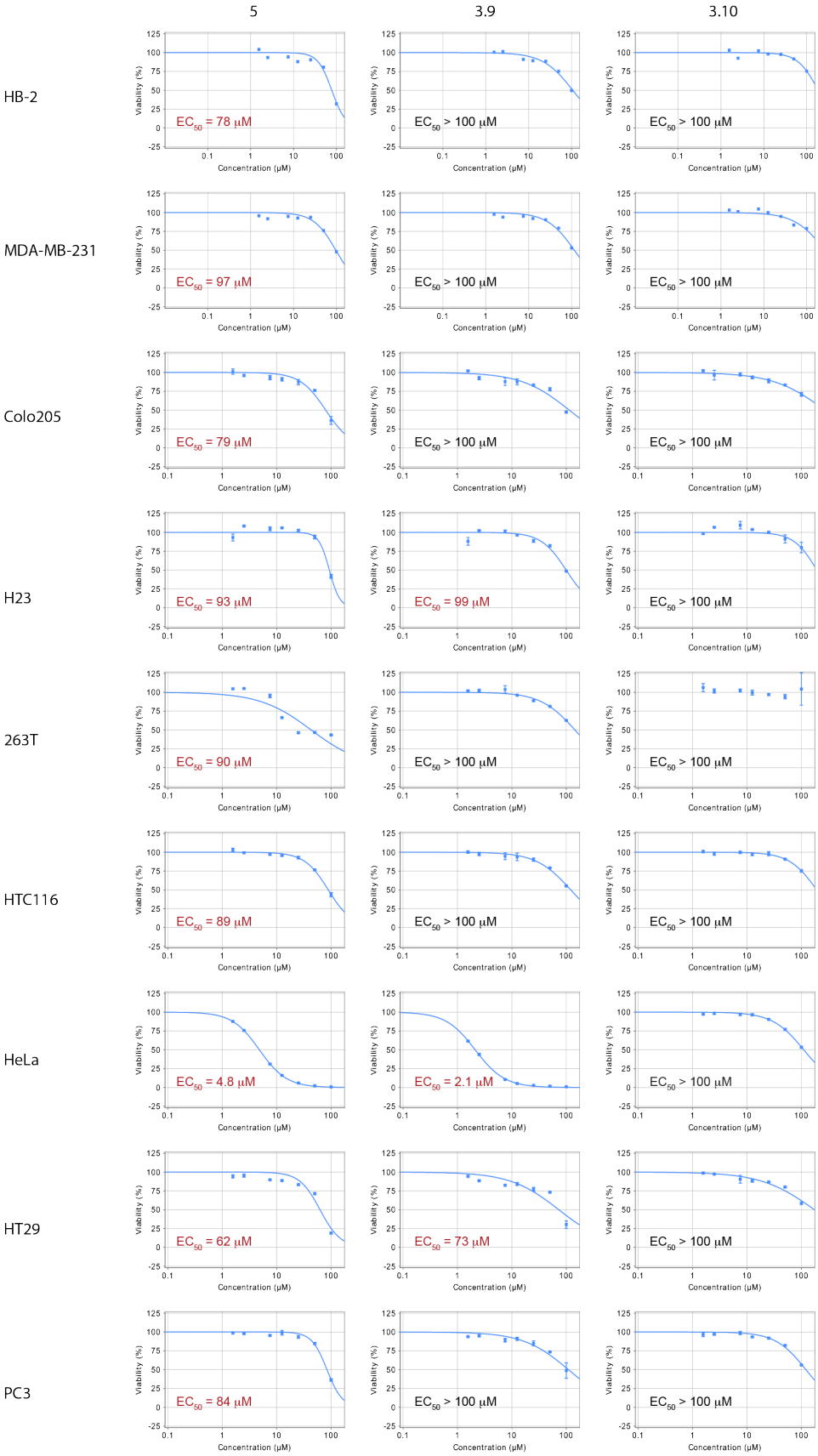

Figure S13. Compounds **5**, **3.9** and **3.10** show little cell toxicity except against HeLa cells. Compounds were incubated for 48 h with seven human cell lines at 7 concentrations up to 100 µM. Cell viability was measured after 48 h using Cell-Titer-Glo assay. The best-fit EC_{50} values are quoted on each plot for single measurements at each concentration for HB-2 and MDA-MB-231 cell lines, and duplicate measurements for the remaining seven cell lines.

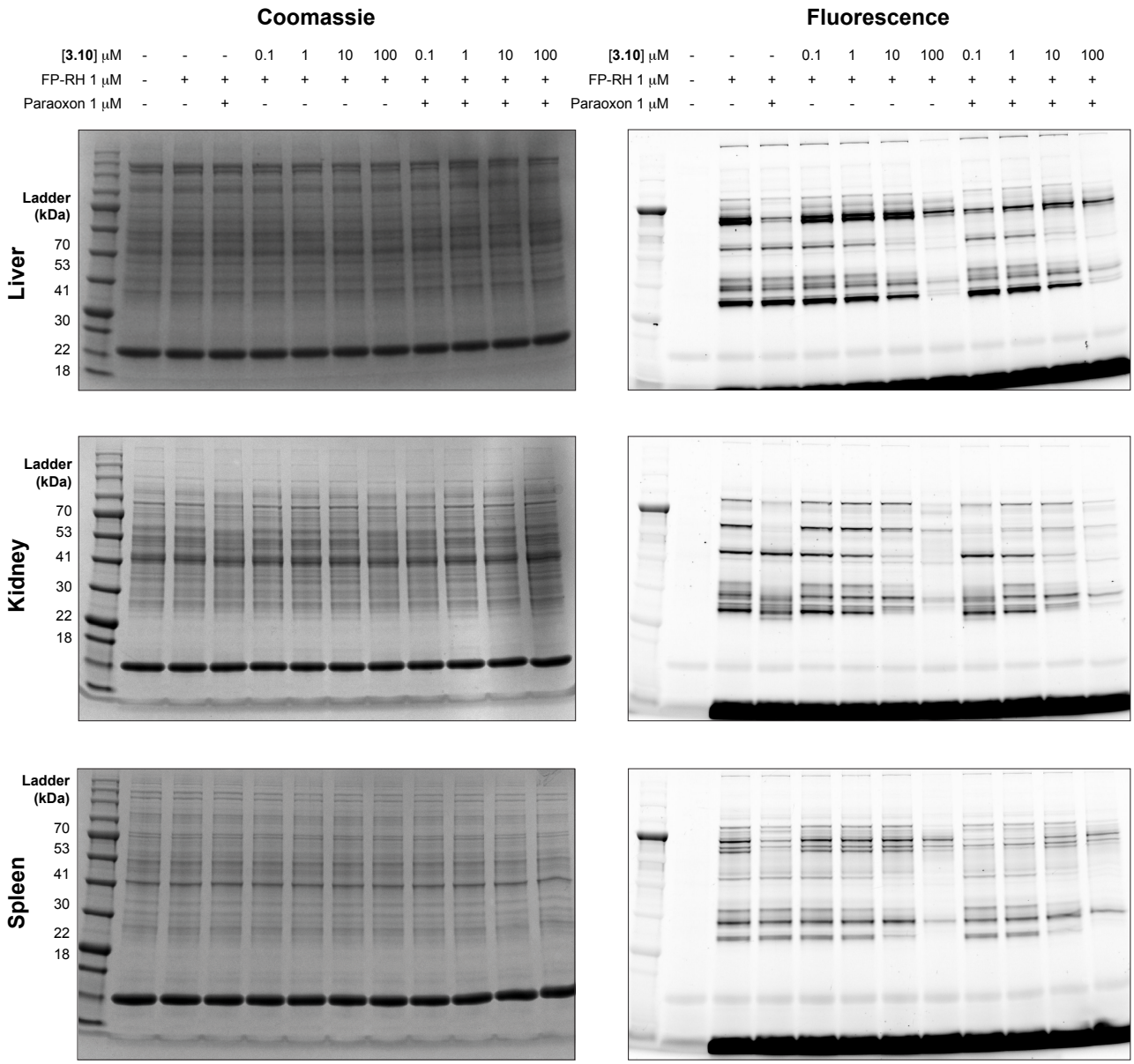

Figure S14. Summary of in-gel fluorescence activity-based protein profiling of serine hydrolases with mouse-tissue derived lysate. Lysates were incubated with a fluorophosphonate-rhodamine (FP-RH) probe, with or without pre-incubation of compound **3.10** or paraoxon (10 minutes; 37°C). The gel for each tissue type was visualized with visible light (left), showing all proteins, and fluorescence (right), showing only proteins labelled with the FP-RH probe.

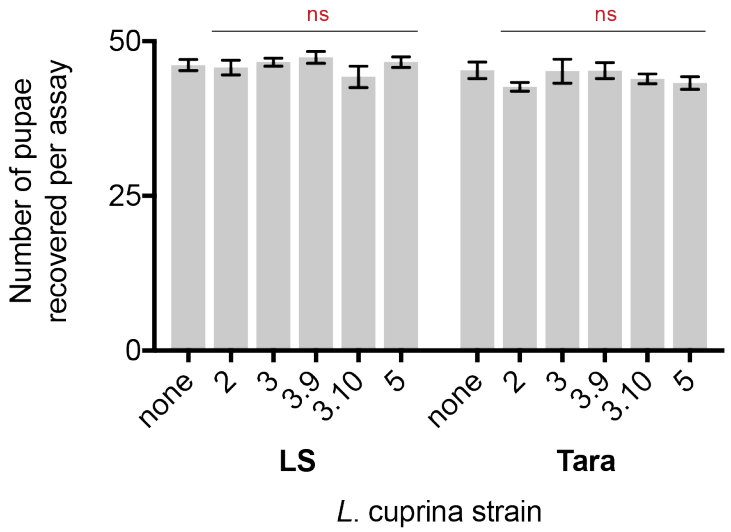

Figure S15. Boronic acid compounds had no effect on *Lucilia cuprina* pupation in the absence of the organophosphates diazinon or malathion. The number of pupae recovered in the absence of boronic acids is compared to the number recovered in the presence of boronic acids at 1 mg per assay for both LS and Tara *L. cuprina* strains. Data is mean ± SEM for three replicate experiments each starting with 50 larvae (ns = not significant; one-way ANOVA to followed by Dunnett's multiple comparison test).

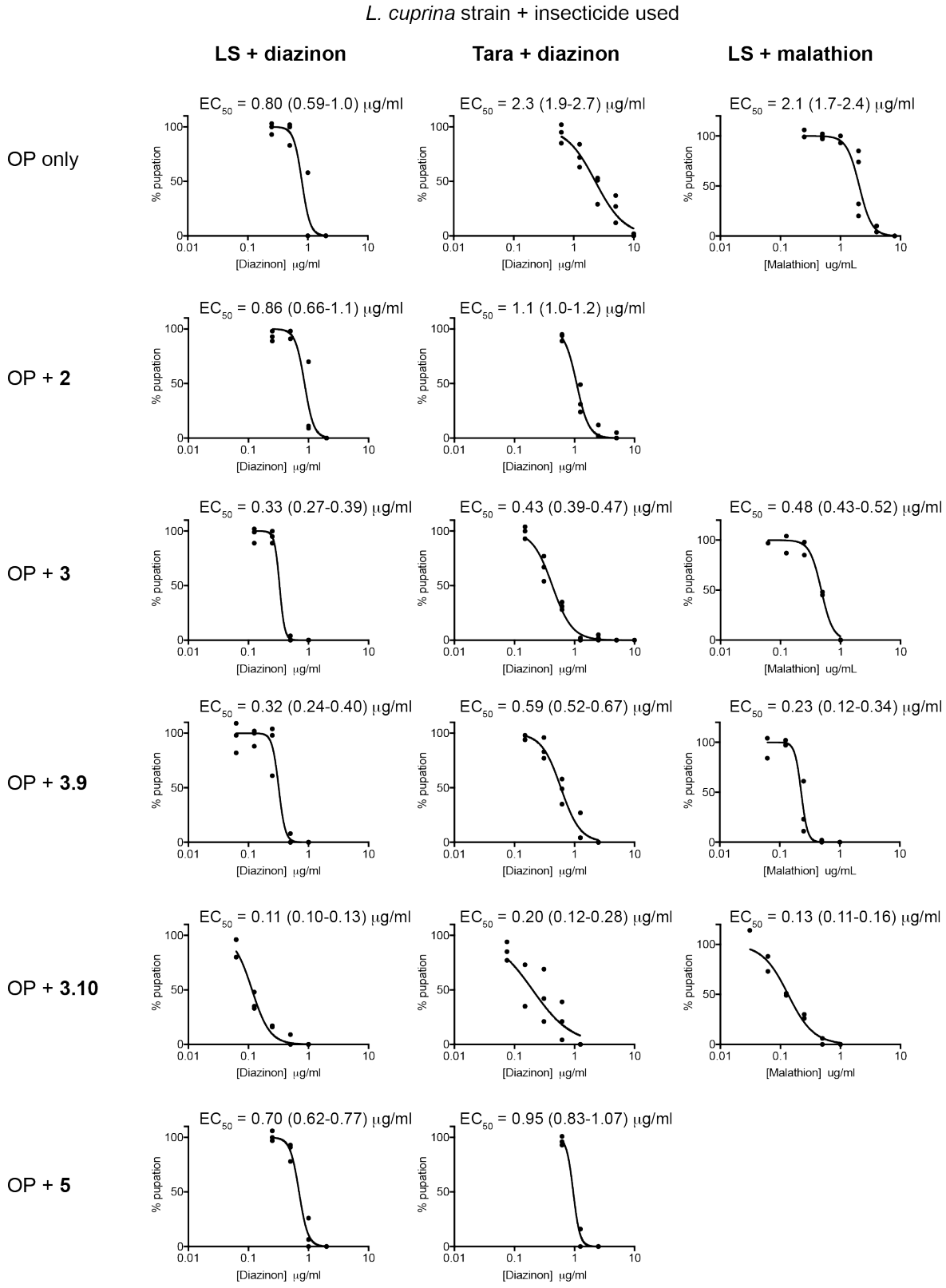

Figure S16. Dose-response curves for *Lucilia cuprina* bioassay. Treatment consisted of organophosphate insecticide only (diazinon / malathion) or insecticide supplemented with boronic acid compound at a set concentration of 1 mg/ml. The concentration of organophosphate insecticide required to reduce the pupation rate by 50% (EC_{50}) was calculated by fitting a sigmoidal dose-response curve to plots of percentage pupation. Each of the data points represents the percentage pupation for 50 initial blowfly larvae with the bioassay repeated three times (diazinon), or two times (malathion), for each concentration of insecticide. The EC_{50} values are presented ± 95% confidence interval.

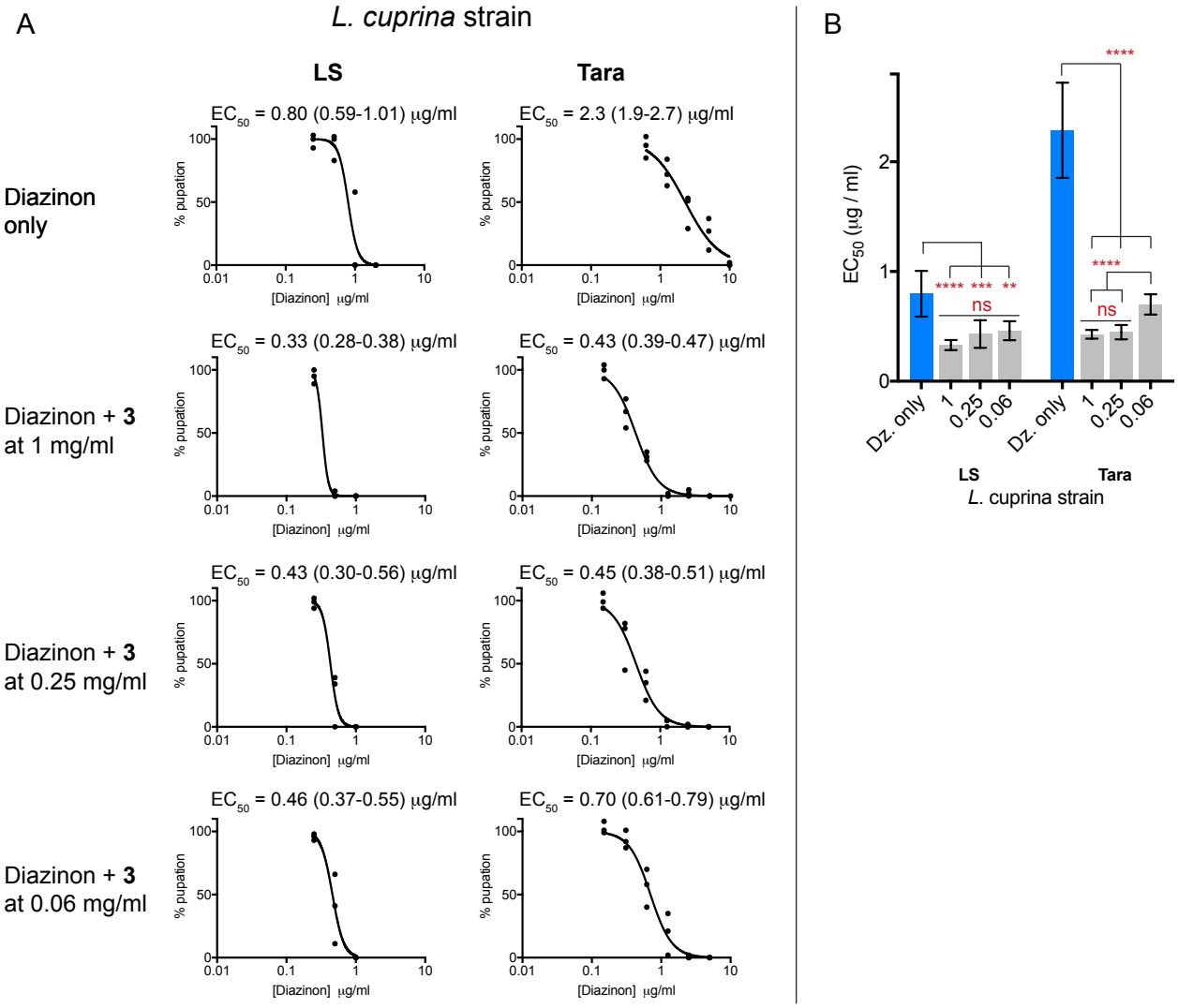

Figure S17. Compound **3** synergizes diazinon against *L. cuprina* at decreased concentrations. *(A)* Dose-response curves for *L. cuprina* bioassays at reduced compound concentration. Treatment consisted of diazinon only, or diazinon supplemented with boronic acid compound at a set concentration of 1, 0.25 or 0.06 mg/ml. The concentration of diazinon required to reduce the pupation rate by 50% (EC_{50}) was calculated by fitting a sigmoidal dose-response curve to plots of percentage pupation. Each of the data points represents the percentage pupation for 50 initial blowfly larvae with the bioassay repeated three times for each concentration of diazinon. The EC_{50} values are quoted as the best-fit value ± 95% confidence interval. *(B)* There was no significant difference between diazinon EC_{50} values when the concentration of compound **3** was reduced to 0.25 and 0.06 mg/ml against the LS blowfly strain, however there was an increase in EC_{50} against the Tara strain when the concentration compound **3** was reduced to 0.06 mg/ml. EC_{50} values are presented ± 95% confidence interval (**P<0.01, ***P<0.001, ns = not significant; one-way ANOVA to followed by Dunnett's multiple comparison test).

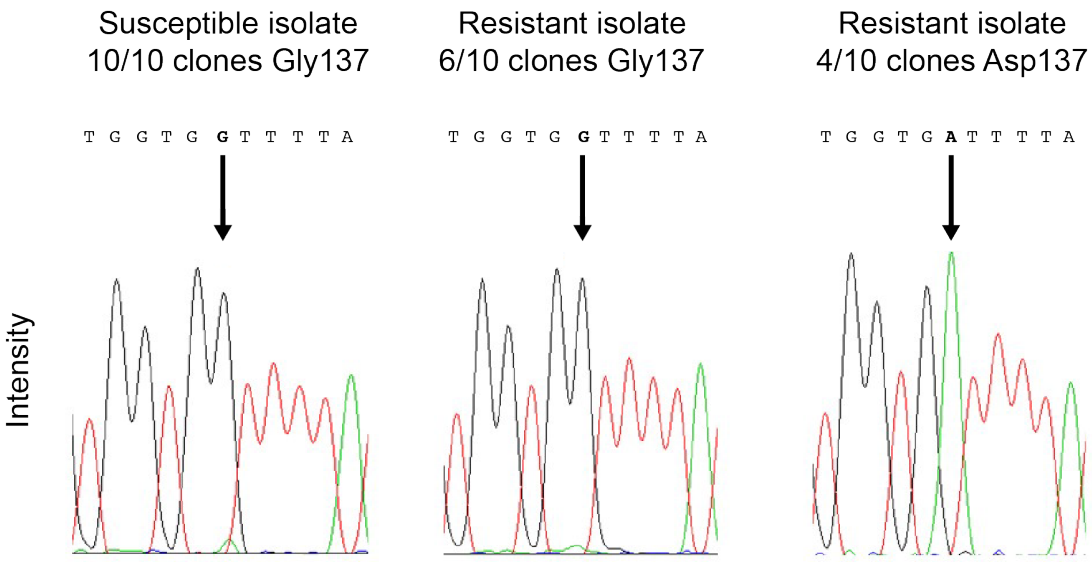

Figure S18. Sequencing of the *Lc*αE7 gene in susceptible (LS) and resistant (Tara) isolates. The susceptible *Lucilia cuprina* stain only carries the wild type αE7 gene, while the resistant strain contains both wild type αE7 (Gly137) and the Gly137Asp variant. Chromatograms and corresponding nucleotides are shown for the relevant region of the αE7 gene.

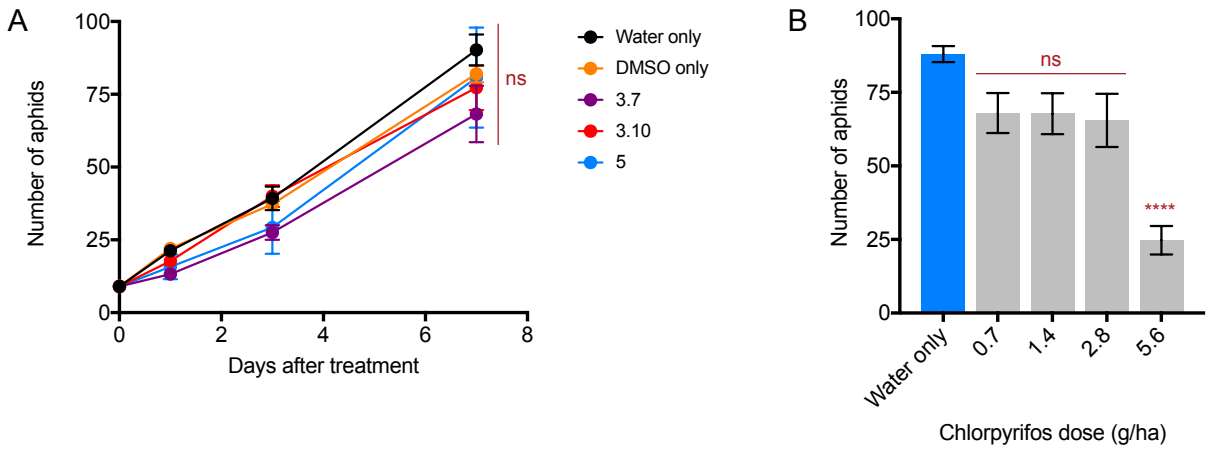

Figure S19. Boronic acid compounds synergize chlorpyrifos against the peach-potato aphid *Myzsus persicae*. *(A)* The boronic acid compounds by themselves had no significant effect on the number of aphids compared to a DMSO only control. Data is mean ± SEM for four repeat experiments (ns = not significant; one-way ANOVA followed by Dunnett's multiple comparison test). *(B)* The effect of chlorpyrifos at four doses seven days after treatment. Only treatment with 5.6 g/ha gave a significant decrease in the number of aphids compared to a water only control (****P<0.0001, ns = not significant; one-way ANOVA followed by Dunnett's multiple comparison test).

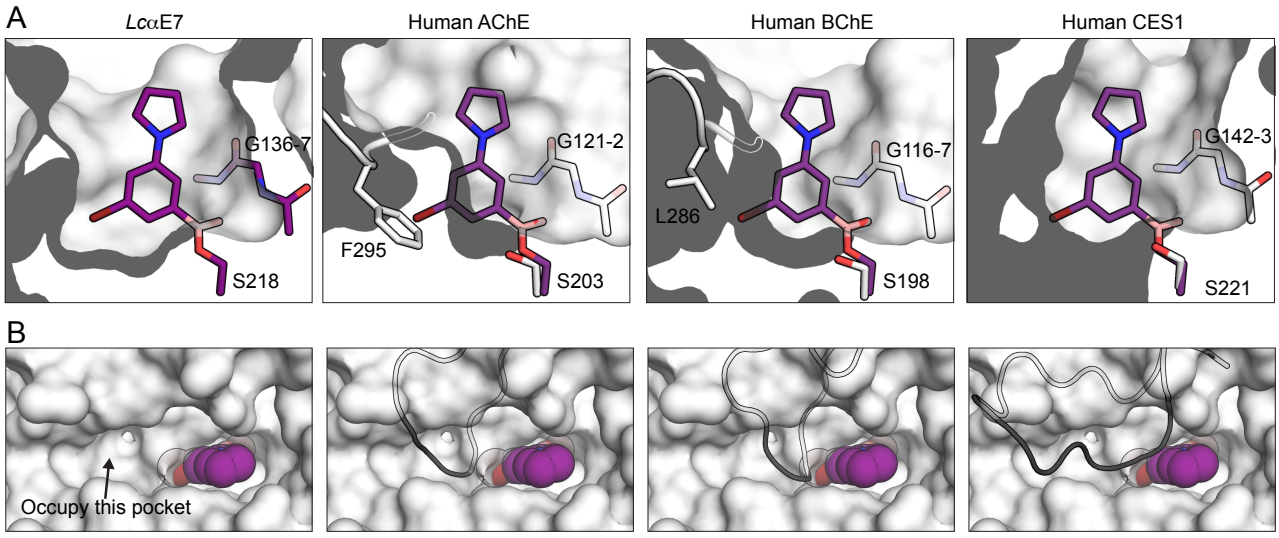

Figure S20. Structural basis for selectivity against human carboxylesterases. *(A)* Sliced-surface view of compound **3** overlaid with human acetylcholinesterase (AChE, PDB code 4EY4 (11)), human butyrylcholinesterase (BChE, 1P0I (12)) and human carboxylesterase 1 (CES1, PDB code 4AB1 (13)). High selectivity against AChE is conferred by a steric clash between Phe295 and the bromo substituent of compound **3**. The enlarged active site of BChE (via replacement of Phe295 with an isoleucine, and a shift in the loop which positions this residue) explains the reduced selectivity of compound **3** against BChE. CES1 has an open active site which allows it to accommodate compound **3**, resulting in low selectivity. *(B)* Surface view of the *Lc*αE7 active site entrance showing a nearby hydrophobic pocket, which if occupied, could confer increased selectivity because of the steric clash with a loop which exists in AChE, BChE and CES1 (black cartoon). Compound **3** is shown as purple spheres.

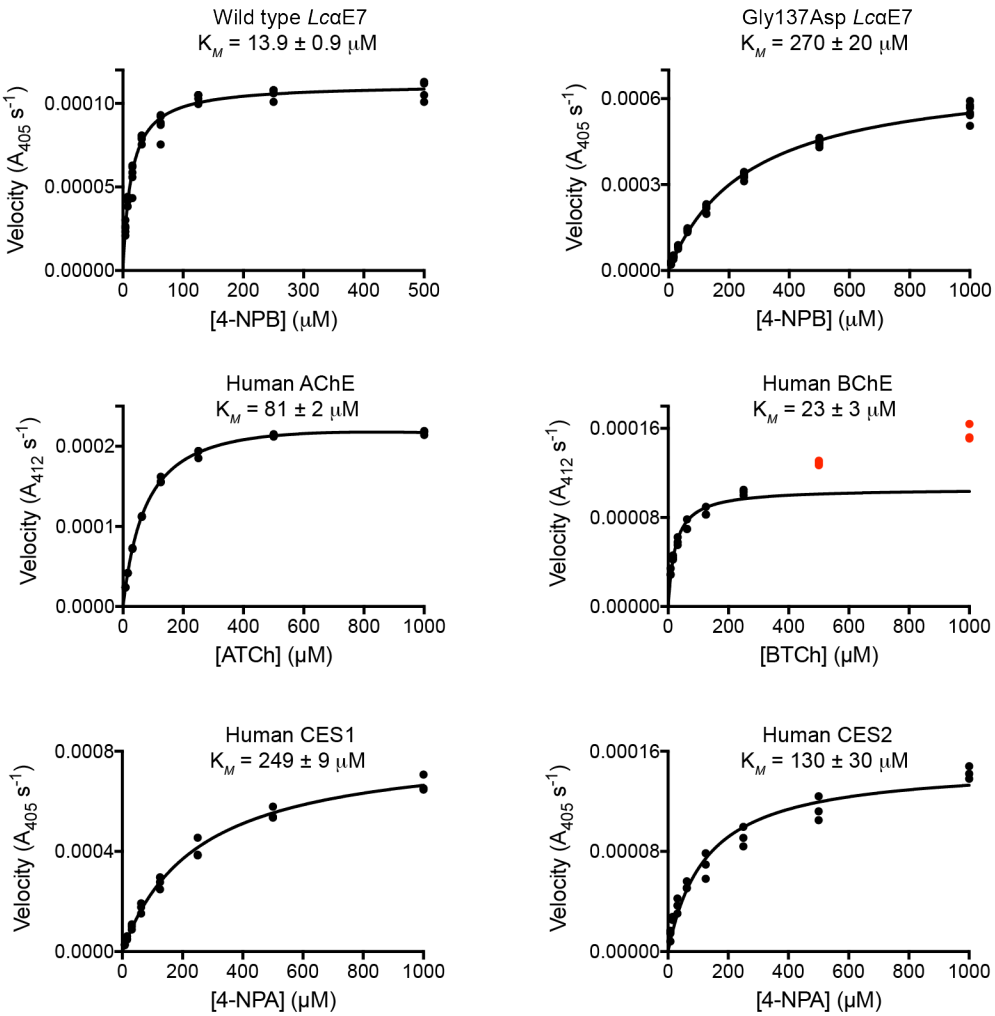

Figure S21. Kinetic parameters for activity assays. Wild type and Gly137Asp *Lc*αE7 were assayed with 4-nitrophenol butyrate (4-NPB), human acetylcholinesterase (AChE) was assayed with acetylthiocholine (ATCh), human butyrylcholinesterase (BChE) was assayed with butyrylthiocholine (BTCh) and human carboxylesterase 1 and 2 (CES1 and CES2) were both assayed with 4-nitrophenyl acetate (4-NPA). Parameters were determined by fitting the Michaelis-Menten equation to plots of enzyme velocity at eight substrate concentrations using non-linear regression. BChE shows activation at high substrate concentrations (14), hence the velocity measurements at 500 and 1000 μM (red dots) were excluded. At least three repeat measurements of enzyme activity were performed for each concentration of substrate. The Michaelis constant (K_M) is presented ± SE.

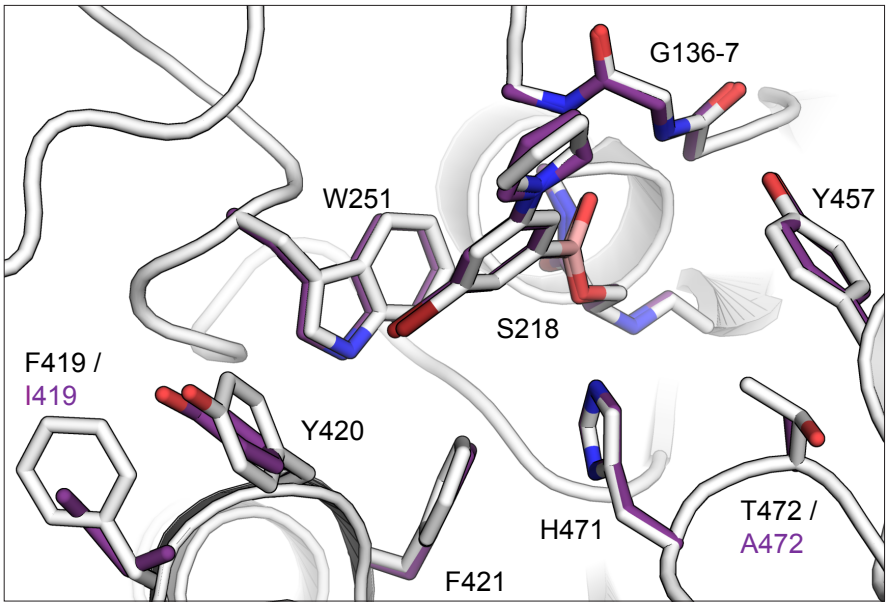

Figure S22. Internal stabilizing mutations present in *Lc*αE7-4a have no effect on boronic acid binding. The co-crystal structure of compound **3** with *Lc*αE7-4a(1) (white sticks, PDB code 5TYN) is aligned with the co-crystal structure of compound **3** with Asp83Ala + Lys530Glu *Lc*αE7 (purple sticks, PDB code 5TYM). The only structural difference is a 30° rotation in the χ_2 dihedral angle of Tyr420 as a result of the Ile419Phe mutation. For clarity, only the backbone of *Lc*αE7-4a is shown (white cartoon).

Table S1. Data collection and refinement statistics.

PDB code (compound)	5TYP (**1**)	5TYO (**2**)	5TYN (**3**)	5TYL (**4**)	5TYK (**5**)	5TYM (**3**)	5TYJ (**3.10**)
Data collection							
Space group	$C222_1$	$C222_1$	$C222_1$	$C222_1$	$C222_1$	$C222_1$	$C222_1$
Cell dimensions							
a, *b*, *c* (Å)	48.46, 101.8, 224.7	49.08, 101.2, 222.8	49.71, 101.07, 222.6	48.77, 101.4, 223.5	47.80, 100.8, 221.8	49.15, 100.8, 224.0	48.58, 102.5, 224.4
α, β, γ (°)	90, 90, 90	90, 90, 90	90, 90, 90	90, 90, 90	90, 90, 90	90, 90, 90	90, 90, 90
Resolution (Å)	1.88 (1.92-1.88)*	1.57 (1.60-1.57)	1.53 (1.56-1.53)	1.75 (1.78-1.75)	1.65 (1.68-1.65)	1.84 (1.88-1.84)	1.75 (1.78-1.75)
R_{merge}	0.16 (2.5)	0.089 (2.7)	0.16 (1.6)	0.14 (2.3)	0.13 (2.2)	0.14 (2.48)	0.12 (3.08)
I / σI	11.9 (1.1)	21.6 (1.0)	6.9 (1.0)	10.3 (0.8)	14.4 (1.3)	12.4 (1.1)	13.3 (0.9)
Completeness (%)	99.9 (98.3)	97.0 (73.8)	99.5 (97.8)	100 (99.9)	100 (99.3)	99.9 (99.9)	100 (100)
Redundancy	13.4 (10.9)	14.3 (11.5)	6.6 (6.9)	7.1 (6.9)	14.0 (13.9)	11.9 (10.9)	14.4 (14.5)
Refinement							
Resolution (Å)	1.88	1.57	1.53	1.75	1.65	1.84	1.75
No. reflections	45621	75341	84196	56360	64943	48767	57007
R_{work} / R_{free}	0.221 / 0.283	0.206 / 0.236	0.193 / 0.233	0.214 / 0.263	0.187 / 0.223	0.228 / 0.287	0.198 / 0.240
No. atoms							
Protein	4567	4571	4614	4565	4572	4564	4579
Ligand/ion	11	17	14	13	18	14	17
Water	129	262	421	194	266	117	205
B-factors							
Protein	40.3	27.4	20.8	30.8	25.6	35.9	39.8
Ligand/ion	36.4	30.0	15.9	26.9	34.0	25.9	29.8
Water	33.6	29.6	27.3	29.7	28.7	30.8	37.9
R.m.s. deviations							
Bond lengths (Å)	0.009	0.007	0.007	0.008	0.007	0.008	0.007
Bond angles (°)	1.2	1.0	1.0	1.1	1.1	1.1	1.0

*Values in parentheses are for highest-resolution shell.

Table S2. *In vitro* inhibition of carboxylesterase enzymes by boronic acid compounds.

	K_i **inhibition constant**[a]					
Compound	Wild type αE7 (**nM**)	G137D αE7 (**nM**)	hAChE (**μM**)	hBuChE (**nM**)	hCES1 (**nM**)	hCES2 (**nM**)
PBA	210 (170-260)	450 (370-550)				
1	12 (9-16)	49 (42-56)	81 (65-100)	260 (220-300)	0.93 (0.84-1.1)	120 (91-160)
2	2.9 (2.2-3.8)	29 (27-32)	63 (50-84)	310 (260-350)	1.4 (1.3-1.6)	9.1 (7.0-12)
3	0.25 (0.22-0.28)	110 (97-130)	25 (20-31)	260 (220-320)	4.1 (3.5-4.9)	21 (15-28)
4	7.2 (6.0-8.7)	190 (160-230)	190 (130-310)	56 (48-66)	1.8 (1.6-2.1)	1100 (900-1500)
5	11 (9-13)	170 (140-190)	26 (21-38)	370 (300-450)	3.4 (3.0-3.9)	59 (45-77)
3.1	0.70 (0.62-0.79)	430 (380-500)				
3.2	0.35 (0.31-0.40)	210 (180-230)				
3.3	0.47 (0.36-0.59)	150 (130-170)				
3.4	3.8 (2.9-4.9)	1000 (900-1200)				
3.5	3.4 (2.6-4.5)	440 (350-550)				
3.6	6.3 (4.5-8.8)	71 (60-85)				
3.7	0.30 (0.26-0.35)	76 (69-85)				
3.8	2.0 (1.7-2.4)	110 (100-120)				
3.9	0.44 (0.39-0.50)	25 (22-27)	14 (10-19)	27 (25-30)	1.1 (1.0-1.2)	2.2 (1.7-2.8)
3.10	0.44 (0.34-0.56)	18 (16-20)	9.3 (11-7.7)	94 (80-110)	1.1 (1.0-1.3)	2.1 (1.6-2.8)
3.11	5.8 (4.1-8.0)	1000 (800-1200)				
3.12	12 (9-16)	1000 (900-1100)				

[a] Inhibition constants are presented with 95% confidence intervals in parentheses. See Fig. S2, S5, S7 and S8 for dose-response curves.

Table S3. Boronic acid compounds are selective over human proteases.

Protease	**3** [a]	**3.9** [a]	**3.10** [a]
DPP4	6	2	-3
DPP8	42	53	37
DPP9	45	75	71
Factor VII	15	26	53
Factor-Xa	53	26	35
Furin	1	-2	-5
GranzymeA	12	23	12
GranzymeB	3	17	11
GranzymeK	5	14	3
HTRA2	23	28	2
Kallikrein11	-71	-148	-43
Kallikrein13	3	-1	0
Matriptase	-1	5	4
Plasma-Kallikrein	6	41	64
Plasmin	13	16	-2
Prolyl Oligopeptidase	61	48	30
PSMB5	3	34	2
PSMB6	16	54	27
PSMB7	39	70	48
PSMB8	19	52	49
PSMB9	12	50	15
PSMB10	43	78	45
Spinesin	26	13	34
Thrombin	32	54	58
tPA	26	40	19
uPA	67	40	32

[a] Average % inhibition of protease at 100 μM of the indicated boronic acid compound (N=2). Inhibition >50% is marked in red.

Table S4. Protease selectivity panel.

Target	Vendor	Lot#	[Enzyme] (nM)	Substrate	Incubation time (hr)
DPP4	ENZO	2021206	0.369	RPAGARK	1.5
DPP8	ENZO	2281220	0.5	RPAGARK	1.5
DPP9	ENZO	7221432	0.3125	RPAGARK	1.5
Factor VII[a]	R&D Systems	NJX0716031	38.6	BOC-VPA-AMC	0.3
Factor Xa	Calbiochem	B76791	20	VMIAALPRTMFIQRR	5
Furin	R&D Systems	INK025061	16	LRRVKRSLDDA	6
Granzyme A	ENZO	11061411	30	PRTLTAKK	5
Granzyme B	ENZO	9161556	0.493	IEPDSGGKRK	5
Granzyme K	ENZO	L27095	40	RPAGARK	5
HTRA2	R&D Systems	HVL1015111	76.1	Casein Fluoroscein	3
Kallikrein 11[b]	R&D Systems	MZV0116081	0.032	BOC-VPA-AMC	3
Kallikrein 13[c]	R&D Systems	NXS0117021	8.9	BOC-VPA-AMC	0.2
Matriptase	R&D Systems	PZZ0916101	0.3134	BOC-QAR-AMC	0.5
Plasma-Kallikrein	R&D Systems	NVH0111081	1.5	ARDIYAASFFRK	1
Plasmin[d]	R&D Systems	MQB0411091	2	KHPFHLVIHTKR	2
Prolyl Oligopeptidase	R&D Systems	QBQ0212011	0.1	VMIAALPRTMFIQRR	2
PSMB5	BOSTON-BIOCHEM	21118515B	0.8	TYETFKSIMKKSPF	1.75
PSMB6	BOSTON-BIOCHEM	21118515B	1	GLTNIKTEEISEVNLDAEFRKKRR	3.75
PSMB7	BOSTON-BIOCHEM	21118515B	0.24	GRSRSRSRSR	2
PSMB8	BOSTON-BIOCHEM	04720017A	0.8	TYETFKSIMKKSPF	4.5
PSMB9	BOSTON-BIOCHEM	04720017A	1	GLTNIKTEEISEVNLDAEFRKKRR	3.75
PSMB10	BOSTON-BIOCHEM	04720017A	2	GRSRSRSRSR	2
Spinesin[b]	R&D Systems	NOS031701A	8.721	BOC-QAR-AMC	0.5
Thrombin	R&D Systems	HWO0413121	1	PRTLTAKK	1.5
tPA	R&D Systems	DATN0212041	9	VMIAALPRTMFIQRR	6
uPA	R&D Systems	HKY0112041	6.5	ADFVRAARR	3

[a] Cascade assay where enzyme was first activated by Thermolysin and then Factor III.

[b] Cascade assay where enzyme was activated by Thermolysin.

[c] Cascade assay where enzyme was activated by Lysyl Endopeptidase.

[d] Cascade assay where enzyme was activated by 0.04x of uPA.

Table S5. Effects of boronic acid compounds on sensitivity of blowfly larvae to diazinon and malathion.

Blowfly strain	Drug treatment[a]	Organophosphate dose response			
		EC_{50}[b] (µg/assay)	95% CI	SR[c]	RR[d]
Laboratory (LS)	Dz. alone	0.80	0.59 – 1.01	-	-
	Dz. plus **2**	0.86	0.66 – 1.06	0.9	-
	Dz. plus **3**	0.33 *	0.27 – 0.39	2.4	-
	Dz. plus **3** (0.25 mg/ml)	0.43 *	0.30 – 0.56	1.9	-
	Dz. plus **3** (0.05 mg/ml)	0.46 *	0.37 – 0.55	1.7	-
	Dz. plus **3.9**	0.32 *	0.25 – 0.40	2.5	-
	Dz. plus **3.10**	0.11 *	0.10 – 0.13	7.3	-
	Dz. plus **5**	0.70	0.62 – 0.77	1.1	-
Field (Tara)	Dz. alone	2.29	1.85 – 2.72	-	2.86
	Dz. plus **2**	1.09 *	0.99 – 1.18	2.1	1.36
	Dz. plus **3**	0.43 *	0.39 – 0.47	5.3	0.54
	Dz. plus **3** (0.25 mg/ml)	0.45 *	0.38 – 0.51	5.1	0.56
	Dz. plus **3** (0.05 mg/ml)	0.70 *	0.61 – 0.79	3.3	0.88
	Dz. plus **3.9**	0.59 *	0.52 – 0.67	3.9	0.74
	Dz. plus **3.10**	0.20 *	0.12 – 0.28	11.5	0.25
	Dz. plus **5**	0.95 *	0.83 – 1.08	2.4	1.19
Laboratory (LS)	Mal. alone	2.06	1.73 – 2.39	-	-
	Mal. plus **3**	0.48 *	0.43 – 0.52	4.3	-
	Mal. plus **3.9**	0.23 *	0.12 – 0.34	9.0	-
	Mal. plus **3.10**	0.13 *	0.11 – 0.16	15.8	-

[a] Diazinon (Dz.) and malathion (Mal.) examined at a range of concentrations in the presence or absence of boronic acid at constant concentration of 1 mg / ml (except where indicated)

[b] * indicates that, within a blowfly strain, EC_{50} for Dz./Mal. plus boronic acid is significantly different from EC_{50} for Dz./Mal. alone (*P<0.0001; one-way ANOVA to followed by Dunnett's multiple comparison test)

[c] SR = synergism ratio = EC_{50} for Dz./Mal. alone / EC_{50} for Dz./Mal. plus boronic acid, within a blowfly strain

[d] RR = resistance ratio = EC_{50} for Dz. alone or Dz. plus boronic acid with the field strain / EC_{50} for Dz. alone for the laboratory strain

SI References

1. Jackson CJ, et al. (2013) Structure and function of an insect α-carboxylesterase (αEsterase7) associated with insecticide resistance. *Proc Natl Acad Sci U S A* 110(25):10177–82.
2. Correy GJ, et al. (2016) Mapping the accessible conformational landscape of an insect carboxylesterase using conformational ensemble analysis and kinetic crystallography. *Structure* 24(6):1–11.
3. Lindquist RN, Terry C (1974) Inhibition of subtilisin by boronic acids, potential analogs of tetrahedral reaction intermediates. *Arch Biochem Biophys* 160:135–144.
4. Tsai IH, Bender ML (1984) Inhibition of porcine elastase and anhydroelastase by boronic acids. *Arch Biochem Biophys* 228:555–559.
5. Garner CW (1980) Boronic acid inhibitors of porcine pancreatic lipase. *J Biol Chem* 255:5064–5068.
6. Takahashi LH, Radhakrishnan R, Rosenfield Jr. RE, Meyer Jr. EF (1989) Crystallographic analysis of the inhibition of porcine pancreatic elastase by a peptidyl boronic acid: structure of a reaction intermediate. *Biochemistry* 28(19):7610–7617.
7. Bone R, Frank D, Kettner C a, Agard D a (1989) Structural analysis of specificity: alpha-lytic protease complexes with analogues of reaction intermediates. *Biochemistry* 28(1983):7600–7609.
8. Koehler KA, Lienhard GE (1971) 2-phenylethaneboronic acid, a possible transition-state analog for chymotrypsin. *Biochemistry* 10(13):2477–2483.
9. Takahashi T, Cheung M, Butterweck T, Schankweiler S, Heller MJ (2015) Quest for a turnover mechanism in peptide-based enzyme mimics. *Catal Commun* 59(2015):206–210.
10. Mabbitt PD, et al. (2016) Conformational disorganization within the active site of a recently evolved organophosphate hydrolase limits its catalytic efficiency. *Biochemistry* 55:1408–1417.
11. Cheung J, et al. (2012) Structures of human acetylcholinesterase in complex with pharmacologically important ligands. *J Med Chem* 55(22):10282–10286.
12. Nicolet Y, Lockridge O, Masson P, Fontecilla-Camps JC, Nachon F (2003) Crystal Structure of Human Butyrylcholinesterase and of Its Complexes with Substrate and Products. *J Biol Chem* 278(42):41141–41147.
13. Greenblatt HM, et al. (2012) Structure of recombinant human carboxylesterase 1 isolated from whole cabbage looper larvae. *Acta Crystallogr Sect F Struct Biol Cryst Commun* 68(3):269–272.
14. Radic Z, Pickering N a., Vellom DC, Camp S, Taylor P (1993) Three distinct domains in the cholinesterase molecule confer selectivity for acetyl- and butyrylcholinesterase inhibitors. *Biochemistry* 32:12074–12084.